Обзор ArXiv/astro-ph, 29 августа-8 сентября 2022

От Сильченко О.К.

ArXiv: 2208.13582

Morphologies of Galaxies at $z \simeq 9 - 17$ Uncovered by JWST/NIRCam Imaging: Cosmic Size Evolution and an Identification of an Extremely Compact Bright Galaxy at $z \sim 12$

Yoshiaki Ono [ID],[1] Yuichi Harikane [ID],[1] Masami Ouchi [ID],[2, 1, 3] Hidenobu Yajima [ID],[4] Makito Abe,[4] Yuki Isobe [ID],[1, 5] Takatoshi Shibuya,[6] Yechi Zhang [ID],[1, 7] Kimihiko Nakajima [ID],[2] and Hiroya Umeda[1, 5]

[1]Institute for Cosmic Ray Research, The University of Tokyo, 5-1-5 Kashiwanoha, Kashiwa, Chiba 277-8582, Japan

[2]National Astronomical Observatory of Japan, 2-21-1 Osawa, Mitaka, Tokyo 181-8588, Japan

[3]Kavli Institute for the Physics and Mathematics of the Universe (WPI), The University of Tokyo, 5-1-5 Kashiwanoha, Kashiwa-shi, Chiba, 277-8583, Japan

[4]Center for Computational Sciences, University of Tsukuba, Ten-nodai, 1-1-1 Tsukuba, Ibaraki 305-8577, Japan
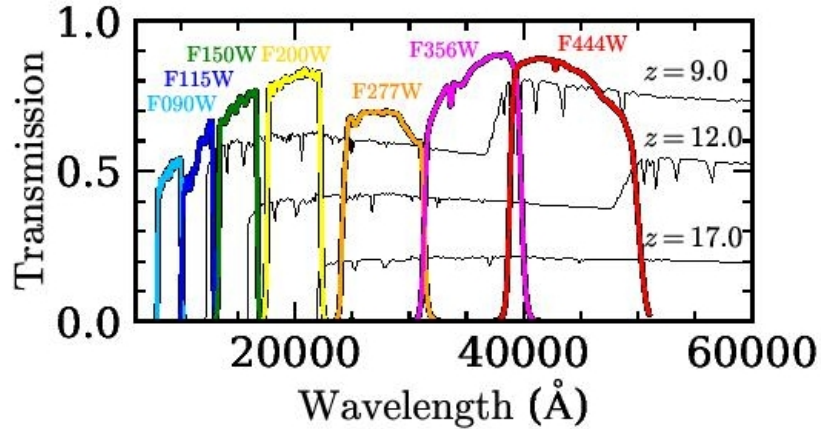
[5]Department of Physics, Graduate School of Science, The University of Tokyo, 7-3-1 Hongo, Bunkyo, Tokyo 113-0033, Japan

[6]Kitami Institute of Technology, 165 Koen-cho, Kitami, Hokkaido 090-8507, Japan

[7]Department of Astronomy, Graduate School of Science, the University of Tokyo, 7-3-1 Hongo, Bunkyo, Tokyo 113-0033, Japan

Первые картинки с JWST

Figure 1. Transmissions of the seven NIRCam broadband filters (cyan: F090W, blue: F115W, green: F150W, yellow: F200W, orange: F277W, magenta: F356W, red: F444W) together with three spectra of star-forming galaxies at $z = 9.0$, 12.0, and 17.0 from the Bruzual & Charlot (2003) library (black lines).

Table 4. Limiting Magnitudes and PSF FWHMs of the JWST NIRCam Images for Size Analysis

| Field | 5σ Depth / 10σ Depth / PSF FWHM | | | |
	F150W	F200W	F277W	F444W
GLASS	29.4 / 28.6 / 0.″0704	29.5 / 28.7 / 0.″0776	—	29.6 / 28.8 / 0.″1605
CEERS	—	29.7 / 28.9 / 0.″0795	29.5 / 28.7 / 0.″1218	—
SMACS J0723	—	29.8 / 29.0 / 0.″0765	—	—
Stephan's Quintet	—	28.0 / 27.2 / 0.″0771	28.7 / 27.9 / 0.″1197	—

NOTE— Limiting magnitudes are measured with randomly distributed 0.″2 diameter circular apertures (Harikane et al. 2022).

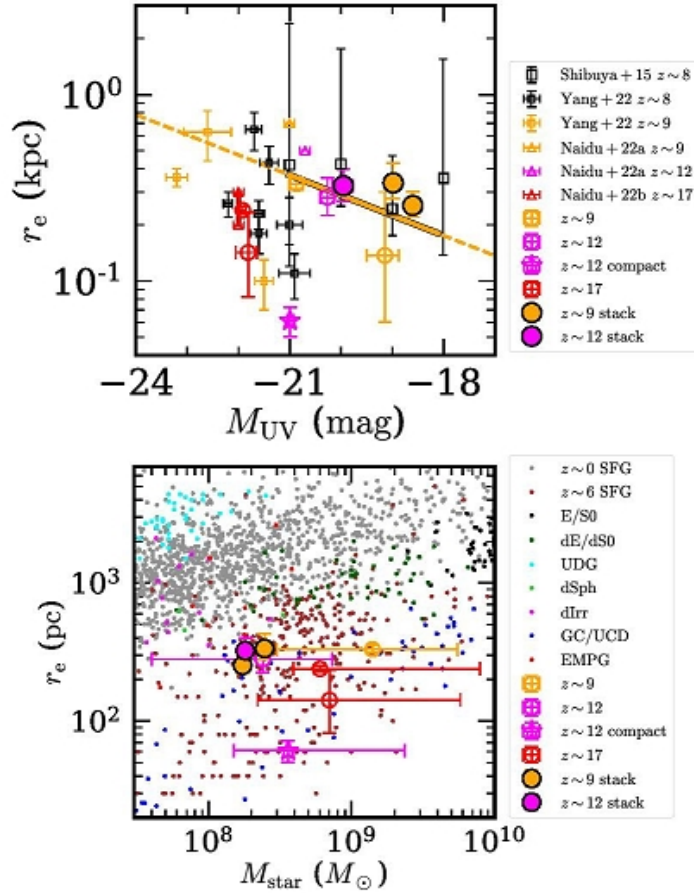# А вот и мордочки (cut 1.5''): image, model, residuals
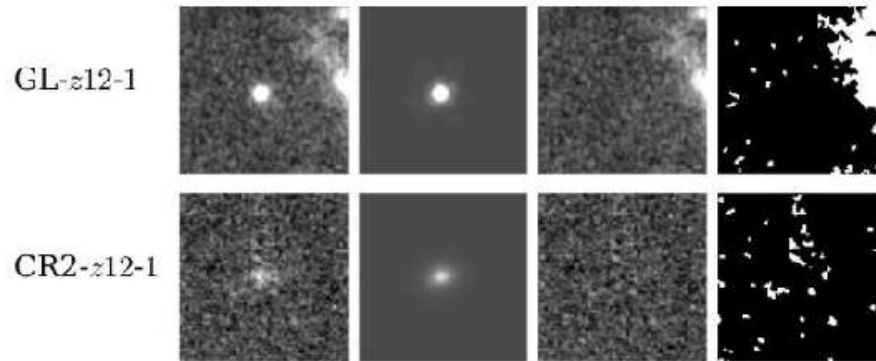
**Figure 9.** Same as Figure 8, but for bright F200W dropouts ($z \sim 12$ galaxy candidates).
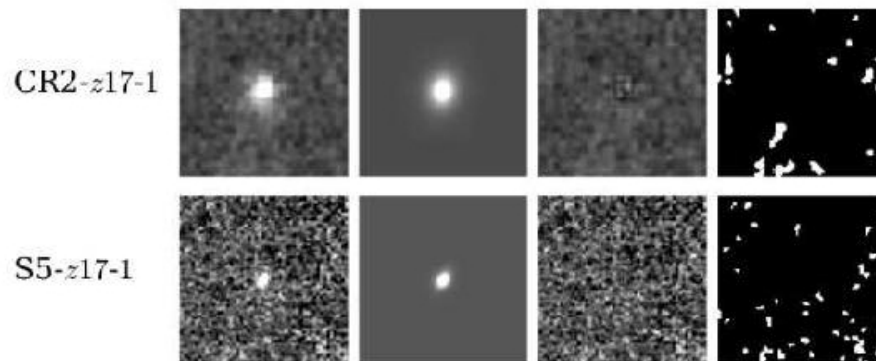
Figure 10. Same as Figure 8, but for bright F277W dropouts ($z \sim 17$ galaxy candidates).

Эволюция размеров

Figure 16. Top: Size–luminosity relation for $z \sim 9$–17 galaxy candidates. The orange, magenta, and red large open circles are bright objects in our $z \sim 9$, $z \sim 12$, and $z \sim 17$ galaxy candidate samples, respectively. The magenta open star denotes the very compact galaxy candidate, GL-z12-1. The orange (magenta) filled circles correspond to the stacked objects of our faint $z \sim 9$ ($z \sim 12$) galaxy candidates, and the orange dashed line is its extrapolation. The orange, magenta, and red small open squares and triangles denote previous JWST results for $z \sim 9$, $z \sim 12$, and $z \sim 17$ galaxy candidates, respectively (Yang et al. 2022; Naidu et al. 2022a; Naidu et al. 2022b). The black large open squares are previous results for $z \sim 8$ galaxy candidates and their large error bars denote the 16th and 84th percentiles of the individual size distribution (Shibuya et al. 2015). The black small open squares are previous JWST results for galaxy candidates at $z < 8.5$ in Yang et al. (2022). **Bottom:** Size as a function of stellar mass for $z \sim 9$–17 galaxy candidates. The large orange, magenta, and red symbols are the same as those in the top panel. The stellar masses of our stacked objects are calculated by using the stellar mass-to-luminosity ratios for the bright candidates. The other small symbols are compiled by Isobe et al. (2021); the gray and brown dots are star-forming galaxies at $z \sim 0$ and $z \sim 6$, respectively (Shibuya et al. 2015; Kikuchihara et al. 2020); the black dots are local ellipticals (E/S0; Norris et al. 2014); the dark green dots are local dwarf ellipticals (dE/dS0; Norris et al. 2014); the cyan dots are local ultra diffuse galaxies (UDGs; van Dokkum et al. 2015; Hashimoto et al. 2020); the light green dots are local dwarf spheroidals (dSph; McConnachie 2012); the magenta dots are local dwarf irregulars (dIrr; McConnachie 2012); the blue dots are globular clusters and local ultra compact dwarfs (GC/UCD; Norris et al. 2014); and the red dots are local extremely metal-poor galaxies (EMPGs; Isobe et al. 2021).
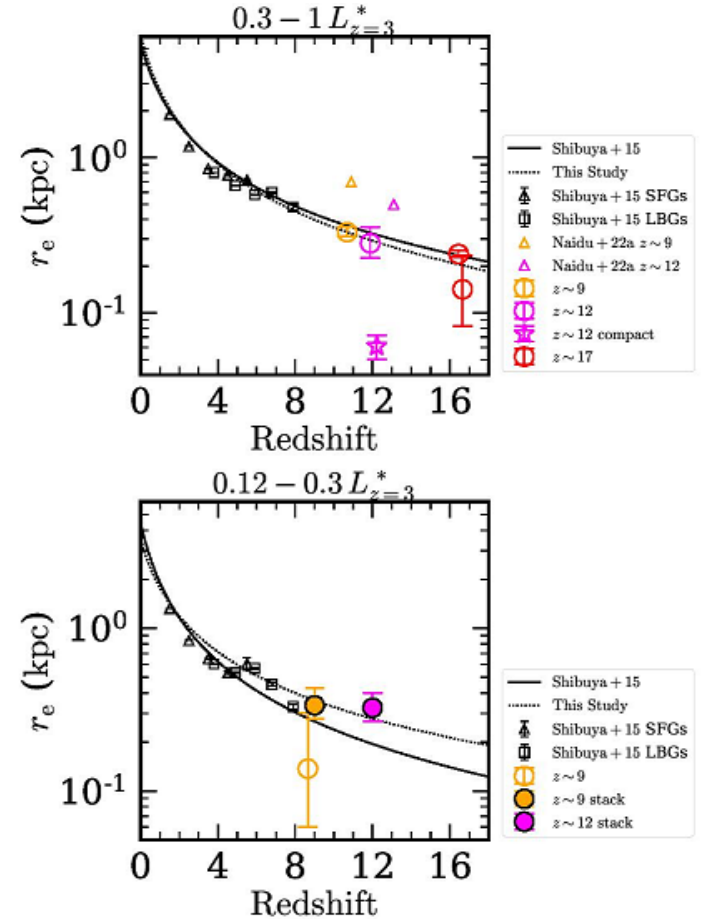
Figure 17. Evolution of the half-light radius of star-forming galaxies with UV luminosities of $(0.3–1)$ $L^*_{z=3}$ (top) and $(0.12–0.3)$ $L^*_{z=3}$ (bottom). The orange, magenta, and red large open circles show bright objects in our $z \sim 9$, $z \sim 12$, and $z \sim 17$ galaxy candidate samples, respectively. The magenta open star denotes the very compact galaxy candidate, GL-z12-1. The orange (magenta) filled circle denotes the stacked object of our faint $z \sim 9$ ($z \sim 12$) galaxy candidates. The orange and magenta small open triangles are previous JWST results for $z \sim 9$ and $z \sim 12$ galaxy candidates, respectively (Naidu et al. 2022a). The black open triangles and squares are previous results for lower-z star-forming galaxies (SFGs) and Lyman break galaxies (LBGs), respectively (Shibuya et al. 2015). The solid and dotted curves correspond to the best-fit functions of $r_e \propto (1+z)^s$ obtained in Shibuya et al. (2015) and in this study, respectively.

Монотонно растет плотность SF!
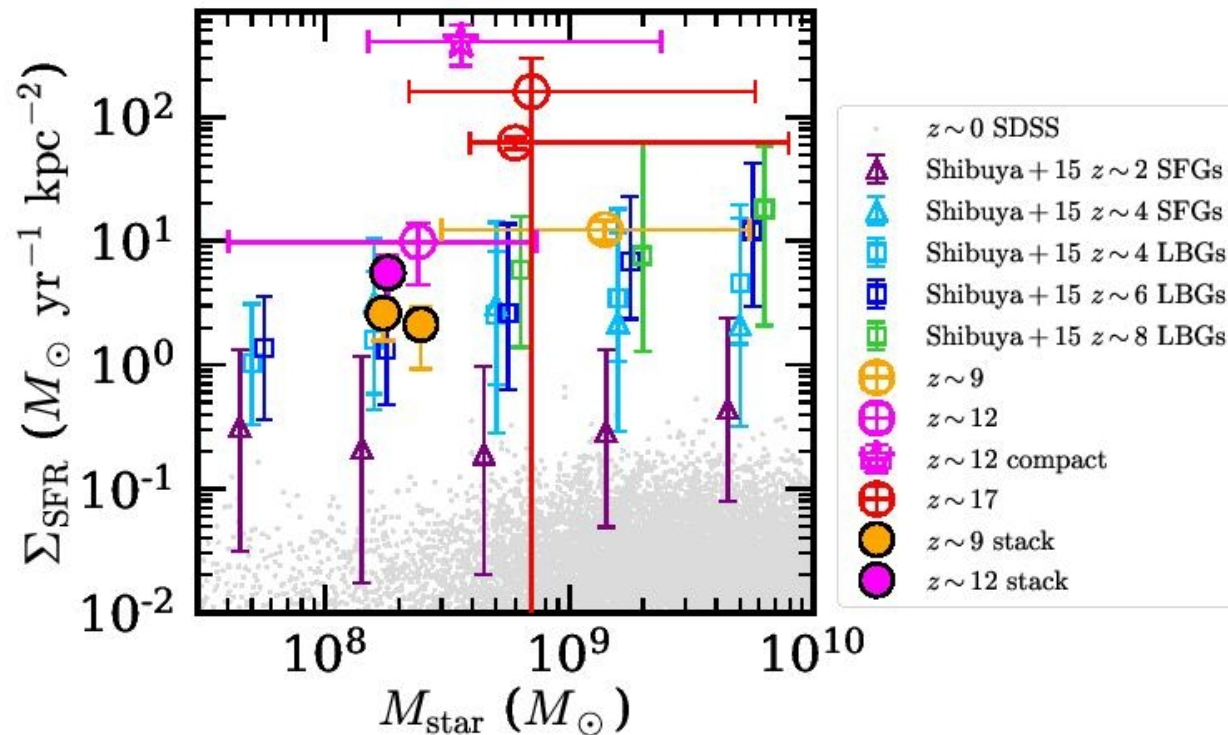
Figure 18. SFR surface density $\Sigma_{\rm SFR}$ vs. stellar mass $M_{\rm star}$. The orange, magenta, and red open circles show bright objects in our $z \sim 9$, $z \sim 12$, and $z \sim 17$ galaxy candidate samples, respectively. The orange (magenta) filled circle denotes the stacked object of our faint $z \sim 9$ ($z \sim 12$) galaxy candidates. The open triangles indicate SFGs at $z \sim 2$ (purple) and $z \sim 4$ (cyan). The open squares denote LBGs at $z \sim 4$ (cyan), $z \sim 6$ (blue), and $z \sim 8$ (green). The gray dots are SDSS galaxies compiled by Shibuya et al. (2015); the $\Sigma_{\rm SFR}$ values are calculated based on the catalog of Lackner & Gunn (2012), and the stellar masses for the SDSS galaxies are taken from Kauffmann et al. (2003), Brinchmann et al. (2004), and Salim et al. (2007).

ArXiv: 2208.14112

The Carnegie-Irvine Galaxy Survey. X. Bulges in Stellar Mass-based Scaling Relations

Hua Gao (高桦) [1,2,3] Luis C. Ho [1,4] AND Zhao-Yu Li [5]

[1] *Kavli Institute for Astronomy and Astrophysics, Peking University, Beijing 100871, China*
[2] *Kavli Institute for the Physics and Mathematics of the Universe (WPI), The University of Tokyo Institutes for Advanced Study, The University of Tokyo, Kashiwa, Chiba 277-8583, Japan*
[3] *Institute for Astronomy, University of Hawaii, 2680 Woodlawn Drive, Honolulu HI 96822, USA*
[4] *Department of Astronomy, School of Physics, Peking University, Beijing 100871, China*
[5] *Department of Astronomy, Shanghai Jiao Tong University, Shanghai 200240, China*

ABSTRACT

We measure optical colors for the bulges of 312 disk galaxies from the Carnegie-Irvine Galaxy Survey and convert their previously available R-band structural parameters to stellar mass parameters. We also measure their average stellar mass surface density in the central $1\,\mathrm{kpc}$ (Σ_1). Comparing the mass-based Kormendy relation with the original one based on flux, we find that the majority of the classifications into classical and pseudo bulges, as well as their overall statistical properties, remain essentially unchanged. While the bulge type classifications of the Kormendy relation are robust against stellar population effects, the mass-based classification criteria do produce better agreement between bulge structural properties and their stellar populations. Moreover, the mass-based Kormendy relation reveals a population of ultra-dense bulges akin to high-z compact early-type galaxies, which are otherwise hidden in the original Kormendy relation. These bulges are probably relics of spheroids assembled in the early Universe, although for some we cannot rule out some contribution from secular growth. We confirm previous studies that Σ_1 correlates well with bulge surface densities.

Поверхностная плотность сфероидов: псевдобалджи диффузны!
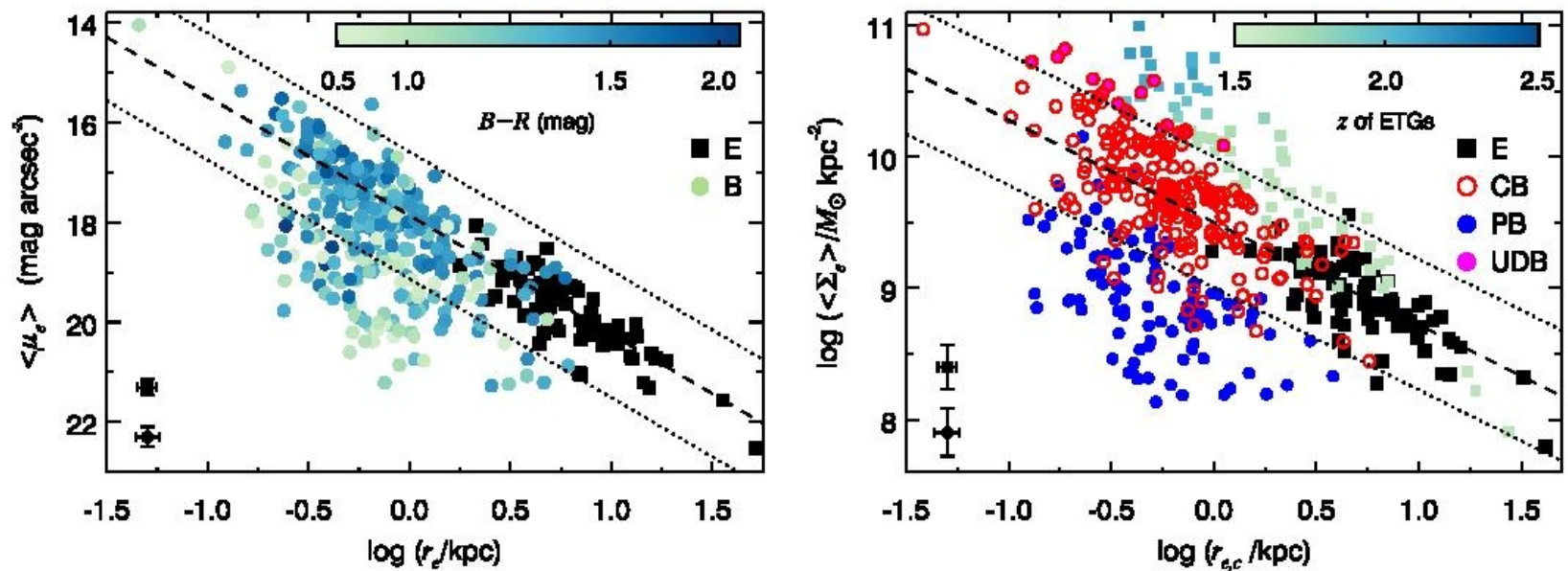
Figure 2. The Kormendy relation of ellipticals and bulges (labeled E and B, respectively), shown in the traditional flux-based units in the R band (left) and stellar mass units (right). The dashed and dotted lines represent the best-fit relation and its 3σ boundary of ellipticals (filled black squares). The filled circles in the left panel are bulges color-coded based on their $B - R$ color. In the right panel, the filled blue circles and open red circles are pseudo bulges (labeled PB) and classical bulges (labeled CB), respectively, classified using the flux-based Kormendy relation; the filled magenta circles are ultra-dense bulges (labeled UDB; Section 4.2.3); the smaller greenish/blueish squares are high-z ETGs color-coded according to their redshift and LOESS-smoothed. Representative error bars are given in the lower-left corner.

Другие популярные критерии хуже для классификации
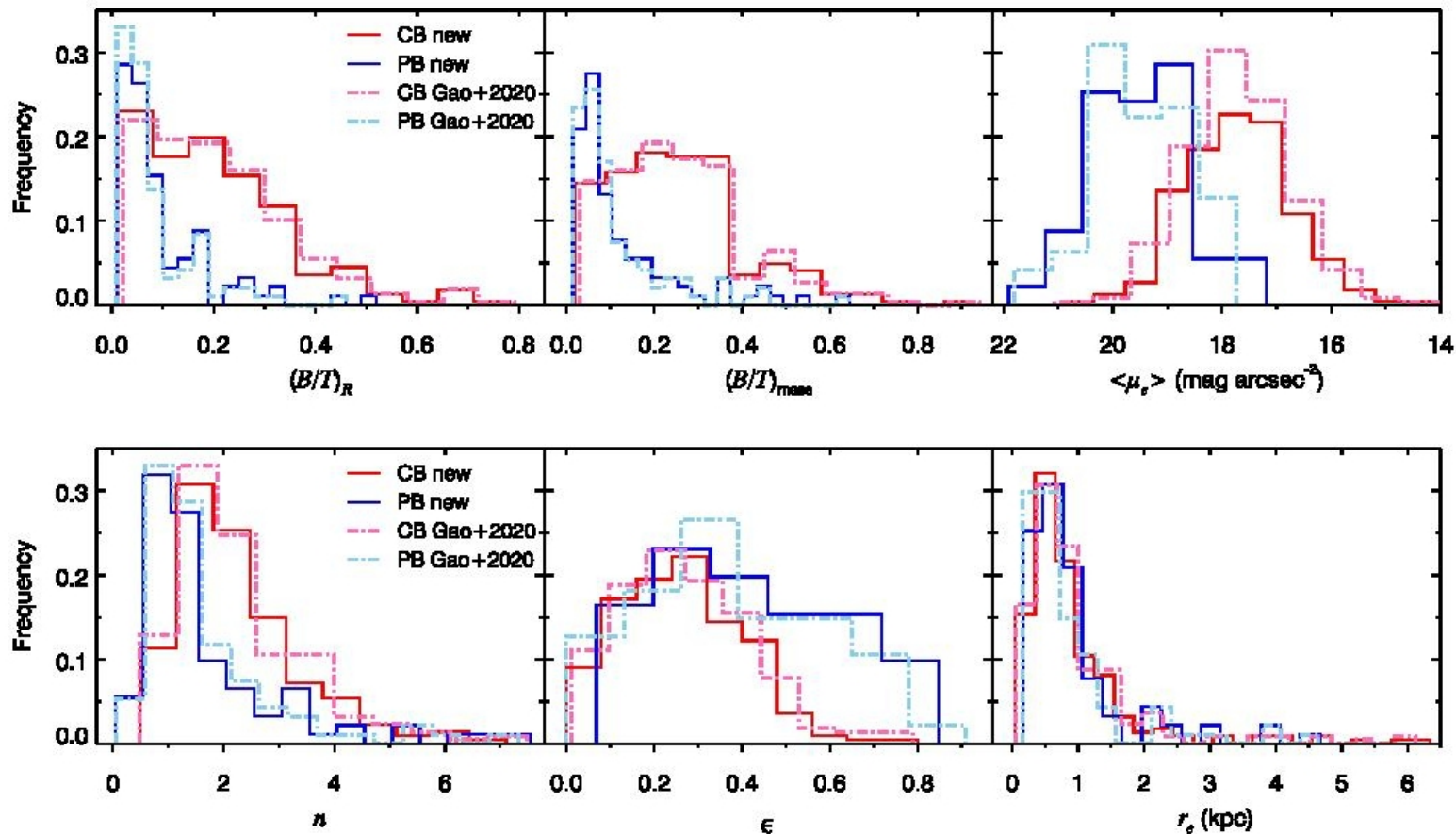
Figure 4. Comparison of structural parameters of classical (reddish) and pseudo (blueish) bulges classified using the original (dot-dashed histograms; Gao et al. 2020) and the new (solid histograms) mass-based Kormendy relation. From left to right, top to bottom, the panels display distributions of R-band bulge-to-total flux ratio, bulge-to-total mass ratio, average effective surface brightness ($\langle \mu_e \rangle$), Sérsic index (n), apparent ellipticity (ϵ), and effective radius (r_e) of the bulge.